

## Accepted Manuscript

Beyond the Standard Two-Film Theory: Computational Fluid Dynamics Simulations for Carbon Dioxide Capture in a Wetted Wall Column

Chao Wang, Zhijie Xu, Canhai Lai, Xin Sun

PII: S0009-2509(18)30151-9  
DOI: <https://doi.org/10.1016/j.ces.2018.03.021>  
Reference: CES 14095

To appear in: *Chemical Engineering Science*

Received Date: 22 December 2017  
Revised Date: 1 March 2018  
Accepted Date: 12 March 2018

Please cite this article as: C. Wang, Z. Xu, C. Lai, X. Sun, Beyond the Standard Two-Film Theory: Computational Fluid Dynamics Simulations for Carbon Dioxide Capture in a Wetted Wall Column, *Chemical Engineering Science* (2018), doi: <https://doi.org/10.1016/j.ces.2018.03.021>

This is a PDF file of an unedited manuscript that has been accepted for publication. As a service to our customers we are providing this early version of the manuscript. The manuscript will undergo copyediting, typesetting, and review of the resulting proof before it is published in its final form. Please note that during the production process errors may be discovered which could affect the content, and all legal disclaimers that apply to the journal pertain.



**Beyond the Standard Two-Film Theory: Computational Fluid Dynamics Simulations for Carbon Dioxide Capture in a Wetted Wall Column**

Chao Wang, Zhijie Xu, Canhai Lai, and Xin Sun

Wang, Chao: Physical and Computational Sciences Directorate, Pacific Northwest National Laboratory, 902 Battelle Blvd, Richland, WA 99354, [chao.wang@pnnl.gov](mailto:chao.wang@pnnl.gov)

Xu, Zhijie: Physical and Computational Sciences Directorate, Pacific Northwest National Laboratory, 902 Battelle Blvd, Richland, WA 99354, [zhijie.xu@pnnl.gov](mailto:zhijie.xu@pnnl.gov)

Lai, Canhai: Computational Eng. & Energy Sciences Division, Oak Ridge National Laboratory, 1 Bethel Valley Rd, Oak Ridge, TN 37830, [laic@ornl.gov](mailto:laic@ornl.gov)

Sun, Xin: Energy and Transportation Science Division, Oak Ridge National Laboratory, 1 Bethel Valley Rd, Oak Ridge, TN 37830, [sunx1@ornl.gov](mailto:sunx1@ornl.gov)

Corresponding Author:

Chao Wang

Pacific Northwest National Laboratory  
902 Battelle Boulevard  
P.O. Box 999, MSIN K7-90  
Richland, WA 99352 USA  
Tel: 509-375-5941  
Fax: 509-372-4720  
[chao.wang@pnnl.gov](mailto:chao.wang@pnnl.gov)

## Beyond the Standard Two-Film Theory: Computational Fluid Dynamics Simulations for Carbon Dioxide Capture in a Wetted Wall Column

Chao Wang, Zhijie Xu, Canhai Lai, and Xin Sun

### Abstract

The standard two-film theory (STFT) is a diffusion-based mechanism that can be used to describe gas mass transfer across liquid film. Fundamental assumptions of the STFT impose serious limitations on its ability to predict mass transfer coefficients. To better understand gas absorption across liquid film in practical situations, a multiphase computational fluid dynamics (CFD) model fully equipped with mass transport and chemistry capabilities has been developed for solvent-based carbon dioxide (CO<sub>2</sub>) capture to predict the CO<sub>2</sub> mass transfer coefficient in a wetted wall column. The hydrodynamics is modeled using a volume of fluid method, and the diffusive and reactive mass transfer between the two phases is modeled by adopting a one-fluid formulation. We demonstrate that the proposed CFD model can naturally account for the influence of many important factors on the overall mass transfer that cannot be quantitatively explained by the STFT, such as the local variation in fluid velocities and properties, flow instabilities, and complex geometries. The CFD model also can predict the local mass transfer coefficient variation along the column height, which the STFT typically does not consider.

**Key words:** computational fluid dynamics, standard two-film theory, carbon capture, physical and chemical absorption, OpenFOAM, wetted wall column

## 1. Introduction

Carbon dioxide (CO<sub>2</sub>) capture from flue gases prevents large amounts of CO<sub>2</sub> from being released into the atmosphere, which is essential in controlling global temperature and avoiding dangerous climate changes<sup>1,2</sup>. Thus, understanding CO<sub>2</sub> absorption in simple chemical devices, for example, a wetted wall column (WWC), is a critical first step for building accurate and reliable numerical models to quantitatively characterize the process of CO<sub>2</sub> absorption, which later can be used as a foundation for complex systems. The standard two-film theory (STFT) is one of the commonly adopted approaches for describing gas absorption in a WWC. In STFT, it is assumed that resistance for mass transfer across the interface between gas and liquid phases is constrained by the thin film closely attached to the interface. The interface itself contains no resistance, and the interfacial concentrations of gas and liquid phases at equilibrium are related by Henry's law. Mass transfer through the films does not change with time and is only controlled by diffusion. Mathematically, when considering a film separating the gas and liquid phases (as shown in Figure 1), Fick's law provides a linear concentration/pressure profile in the film, and the flux  $J$  can be expressed as<sup>3</sup>

$$J = k_L(C_i - C) = k_g(p - p_i), \quad (1)$$

where  $C_i$  is liquid interface concentration,  $C$  is the bulk liquid concentration,  $p_i$  is gas interface pressure,  $p$  is the bulk gas pressure,  $k_L$  (m/s) is the liquid phase mass transfer coefficient, and  $k_g$  (mol/(Pa·s·m<sup>2</sup>)) is the gas phase mass transfer coefficient. Henry's constant can be used to relate liquid concentrations to their equivalent equilibrium gas partial pressures, so the liquid film flux can be expressed in terms of partial pressure. As a result, the middle section of equation (1) also can be expressed as

$$k_L(C_i - C) = k'_i(p_i^* - p^*), \quad (2)$$

where  $p_i^*$  is the converted equilibrium partial pressure from liquid concentrations at the interface,  $p^*$  the converted bulk liquid equilibrium partial pressure, and  $k'_l = k_L/H$ . Here,  $H$  is the Henry's constant ( $\text{Pa}\cdot\text{m}^3/\text{mol}$ ). If there are chemical reactions occurring between gas and liquid phases, then  $k'_l = k_L E/H$ , where  $E$  is the enhancement factor defined as the ratio of flux with chemical reactions to that without chemical reactions. After, the flux across the entire film can be expressed in terms of the overall mass transfer coefficient,  $K_G$ , as follows:

$$J = K_G(p - p^*). \quad (3)$$

From the preceding equations, the expression of STFT can be introduced as

$$\frac{1}{K_G} = \frac{1}{k_g} + \frac{1}{k'_l}. \quad (4)$$

Traditional/empirical correlations often are selected to predict the gas and liquid phase mass transfer coefficients in a WWC for reactive  $\text{CO}_2$ /monoethanolamine (MEA) systems. For example, the gas film mass transfer coefficient is commonly determined using the work from Pacheco et al. <sup>4</sup>:

$$k_g = \frac{ShD}{RTd}, \quad (5)$$

where  $D$  is diffusivity,  $R$  is the gas constant,  $T$  is temperature,  $d$  is hydraulic diameter, and  $Sh$  is the Sherwood number that can be expressed as

$$1.075 \left[ ReSc \left( \frac{d}{h} \right) \right]^{0.85}. \quad (6)$$

Here,  $Re$  is the Reynolds number,  $Sc$  is the Schmidt number, and  $h$  is the WWC length.

The liquid film mass transfer coefficient is analytically approximated using Dugas' work <sup>5</sup>:

$$k_L = \left( \frac{3^{1/3} 2^{1/2}}{\pi^{1/2}} \right) \left( \frac{Q^{1/3} h^{1/2} W^{2/3}}{A} \right) \left( \frac{g\rho}{\mu} \right)^{1/6} D^{1/2}, \quad (7)$$

where  $Q$  is solvent volumetric flow rate,  $W$  is circumference of the WWC,  $A$  is the gas-liquid contact area,  $g$  is the gravitational constant,  $\rho$  is density, and  $\mu$  is dynamic viscosity.

The enhancement factor is normally determined from Dang and Rochelle's work <sup>6</sup>:

$$\frac{1}{E} = \frac{1}{E_l} + \frac{1}{E_{inst}}, \quad (8)$$

where  $E_l$  is the pseudo-first-order enhancement factor and  $E_{inst}$  is the instantaneous enhancement factor. Specifically,  $E_l$  can be derived by shell balance:

$$E_l = \frac{\sqrt{k_{MEA} C_{MEA,bulk} D_{CO_2}}}{k_L}, \quad (9)$$

where  $k_{MEA} \left( \frac{m^3}{mol \cdot s} \right) = 0.001 * 10^{10.99 - 2152/T(K)}$ ,  $C_{MEA,bulk}$  is bulk MEA concentration, and  $D_{CO_2}$  is the diffusivity of CO<sub>2</sub> in MEA. The estimation of  $E_{inst}$  can be expressed as

$$E_{inst} = C_{MEA,total} H_{CO_2}^{pc} \frac{\partial(\text{loading})}{\partial P_{CO_2}^*} \sqrt{\frac{D_{CO_2}}{D_{product}}}, \quad (10)$$

where  $C_{MEA,total}$  is total MEA concentration,  $H_{CO_2}^{pc}$  is the Henry's constant in the unit of m<sup>3</sup>/(mol·Pa), and  $\frac{D_{CO_2}}{D_{product}} \approx 2$ ,  $\frac{\partial(\text{loading})}{\partial P_{CO_2}^*}$  is obtained from the vapor-liquid equilibrium model <sup>6</sup>.

However, for CO<sub>2</sub> loading less than 0.3,  $\frac{\partial(P_{CO_2}^*)}{\partial \text{loading}} \approx 0$ .

To apply the STFT to predict overall mass transfer, several assumptions are satisfied and/or approximately satisfied: 1) the species concentrations at any locations do not change with time, 2) laminar film exists at the interface on both the gas and liquid sides, and 3) equilibrium at the interface is achieved instantaneously such that the interface has negligible resistance. However, there are many real-world gas absorption applications where these assumptions can hardly be satisfied. First of all, the variation of gas and liquid velocity and fluid properties often changes with locations. For example, for a high gas injection flow rate, the gas phase mass transfer resistance may vary spatially depending on the local flow regime, i.e., laminar, transitional, or turbulent flow, within the large-scale absorber. In addition, for gas absorption using non-aqueous or water-lean solvents, the local solvent properties (for example, diffusivity and viscosity) may

be significantly affected by CO<sub>2</sub> loading, which, in turn, leads to a large variation of mass transfer coefficients at different locations. These local changes to flow behavior and fluid properties cannot be accurately captured in a simple STFT. Second, flow instabilities, for instance, induced oscillating solvent injection, may lead to waves on the film surface along a falling film. In such cases, variation in the film thickness may have a substantial effect on the mass transfer coefficient that is not well represented by a STFT. Finally, multidimensional structured or random packings typically are used in large-scale carbon capture devices. The complex packing structure may produce a large variation in film thickness, solvent properties, and create a complex flow field—all of which will have significant impact on the overall mass transfer coefficient. However, the STFT model is developed on a one-dimensional basis. Hence, it cannot fully characterize the complex behavior in real applications.

Given these disadvantages, some theories/models have been developed by generalizing STFT. The penetration theory<sup>7</sup> defines the flux to be proportional to  $\sqrt{D/t}$ , where  $D$  is diffusivity and  $t$  is time. The surface renewal theory<sup>8</sup> describes the flux as proportionate to  $\sqrt{Dr}$ , and  $r$  is a term representing how fast the surface is renewed. The boundary layer theory<sup>9</sup> predicts the mass transfer coefficient for a well-developed laminar film to be proportional to  $D^{2/3}$ . In contrast to the simple STFT, these mass transfer models are more advanced. However, they still are unable to capture the effects of all variations on the mass transfer coefficient in real applications that are strongly influenced by local variations of fluid velocities, physical properties, and different flow regimes.

In efforts to better understand the effects of these key factors that may occur in real-world gas absorption scenarios, the use of computational fluid dynamics (CFD) modeling tools has surged. A number of research works focusing on numerical simulations of mass transfer can be

found in the literature<sup>10-16</sup>. Among them, the volume of fluid (VOF) method with the continuum surface force (CSF) model<sup>17,18</sup> has become a typical approach to study the hydrodynamics of gas-liquid flow that explicitly tracks the gas-liquid interface. In addition, the one-fluid formulation that accounts for diffusion, advection, and chemical reactions often is used to describe the flow and chemical kinetics<sup>19</sup>. In this study, a CFD model that uses the VOF and one-fluid formulation is developed to simulate solvent-based carbon capture, namely, CO<sub>2</sub> physical absorption and chemical removal in a WWC. The numerical prediction of mass transfer coefficient can naturally account for the dependence on the local variation of fluid velocities and properties, flow instabilities, and geometric factors. The purpose of this work is to establish a multiphase CFD model fully equipped with mass transport and chemistry capabilities as a solid framework to predict the CO<sub>2</sub> mass transfer across liquid film, which exceeds the limits of STFT. In this paper, Section 2 introduces the framework of CFD modeling, while simulation results and discussions are described in Section 3. Section 4 features the concluding remarks.

## 2. Framework of Numerical Modeling

### 2.1 Governing Equations

A VOF model is employed to solve for two Newtonian, incompressible, isothermal, and immiscible fluid flows by tracking the volume fraction ( $\alpha_i$ ) of each phase ( $l$  represents liquid phase, while  $g$  represents gas phase) in the volume fraction equation. The volume fraction equation is introduced as

$$\frac{\partial}{\partial t}(\alpha_L) + \nabla \cdot (\alpha_L \mathbf{u}) = 0, \quad (11)$$

where  $\mathbf{u} = (u, v)$  denotes the velocity vector with components in  $x$  and  $y$  directions, respectively.

The volume fraction of gas phase  $\alpha_g$  can be computed as

$$\alpha_g = 1 - \alpha_L. \quad (12)$$

The continuity and Navier-Stokes equations are given as

$$\frac{\partial \rho}{\partial t} + \nabla \cdot (\rho \mathbf{u}) = 0, \quad (13)$$

$$\frac{\partial}{\partial t} (\rho \mathbf{u}) + \nabla \cdot (\rho \mathbf{u} \mathbf{u}) = -\nabla p + \nabla \cdot [\mu (\nabla \mathbf{u} + \nabla \mathbf{u}^T)] + \rho \mathbf{g} - \mathbf{F}_{st}, \quad (14)$$

where density  $\rho$  and viscosity  $\mu$  can be defined in a volume fraction averaged form as

$$\rho = \alpha_L \rho_L + \alpha_g \rho_g, \quad (15)$$

$$\mu = \alpha_L \mu_L + \alpha_g \mu_g. \quad (16)$$

The surface tension force,  $\mathbf{F}_{st}$  in Eq. (14), can be expressed using the CSF model proposed by Brackbill et al.<sup>20</sup>,

$$\mathbf{F}_{st} = \frac{\sigma_{st} \rho \kappa \nabla \alpha_L}{2(\rho_L + \rho_g)}, \quad (17)$$

where  $\sigma_{st}$  is the surface tension coefficient,  $\kappa = -\nabla \cdot \tilde{\mathbf{n}}$  represents the curvature of the surface, and  $\tilde{\mathbf{n}}$  is the unit interface normal vector that can be defined as

$$\tilde{\mathbf{n}} = \frac{\mathbf{n}}{|\mathbf{n}|}, \quad (18)$$

where  $\mathbf{n} = (n_x, n_y) = -\nabla \alpha_L$  is the vector along the interface normal.

The one-fluid formulation for the transport of chemical species is adopted here to explicitly model advection, diffusion, interfacial mass transport<sup>19</sup>, and chemical reactions with one equation for two phases.

$$\frac{\partial c_i}{\partial t} + \nabla \cdot (\mathbf{u} c_i - D_i \nabla c_i - \Gamma_i) - W_i = 0, \quad (19)$$

where

$$\Gamma_i = -D_i \frac{c_i(1-k_i)}{\alpha_L + k_i(1-\alpha_L)} \nabla \alpha_L,$$

$$D_i = \frac{D_{i,L} D_{i,g}}{\alpha_L D_{i,g} + (1-\alpha_L) D_{i,L}}.$$

Here,  $c_i$  represents the concentration for species  $i$ . The diffusivity  $D_i$  is computed using the harmonic average. The term  $\Gamma$  in Eq. (19) accounts for the discontinuity between two phases with  $\Gamma$  approaching zero for  $k_i = 1$  (same solubility in both phases).  $k_i = c_{i,g}^I/c_{i,L}^I$  denotes the dimensionless Henry's constant, and  $c_{i,g}^I$  and  $c_{i,L}^I$  are the gas- and liquid-phase concentrations of species  $i$  at the gas-liquid interface. The last term  $W_i$  is the production term that models the chemical reactions. Note that  $W_i$  equals zero for physical absorption only. For  $\text{CO}_2$  absorbed by MEA, the reaction term can be expressed as<sup>21-25</sup>

$$W_{\text{CO}_2} = r(c_{\text{CO}_2} - c_{\text{CO}_2(aq)})c_{\text{MEA}}\alpha_L, \quad (20)$$

where the reaction rate constant  $r$  ( $\text{m}^3/\text{mol/s}$ ) can be calculated based on a regression model using the data obtained by Ali<sup>26</sup>:

$$\ln r = 20.54 - \frac{5612.91}{T}. \quad (21)$$

Here,  $T$  is the temperature. The equilibrium aqueous  $\text{CO}_2$  concentration dissolved in MEA solution,  $c_{\text{CO}_2(aq)}$  from Eq. (20), can be computed as<sup>27</sup>

$$c_{\text{CO}_2(aq)} = \left(30.96 - \frac{10584}{T} - 7.187\theta\varphi\right) \frac{\theta^2}{(1-2\theta)^2} \frac{1}{k_{\text{CO}_2}RT}, \quad (22)$$

where  $\theta$  is the  $\text{CO}_2$  loading,  $\varphi$  is the MEA molar fraction, and  $R$  is the gas constant.

Note that the system is assumed to operate under an isothermal condition. Therefore, the temperature maintains uniform in the column and the value can be obtained from the corresponding experimental settings in Table 2 column 7. In the future study, energy conservation equation will be explicitly solved to account for the impact of heat generation due to chemical reactions on mass transfer coefficient.

## 2.2 Geometry and Boundary Conditions

Figure 2 shows a two-dimensional countercurrent gas flow geometry to model a typical WWC with solvent falling down the vertical wall and gas moving up. The solvent inlet and outlet are respectively located at the top-left and bottom-left corners, while the gas inlet and outlet are located at the bottom-right and top-right corners. The column has a height of 90.9 mm and a width of 5.25 mm. Both the inlet and outlet are 1 mm in size.

The boundary conditions for the left, right, bottom, and top walls are set to be a non-slip condition. At the solvent inlet, flow velocity and the concentrations of solvent species are given together. At the solvent outlet, the concentration gradient ( $dc/dy$ ) is prescribed at zero because the flow is assumed to be fully developed<sup>17</sup>. For the gas inlet, concentrations of gas species, as well as the gas inlet velocity, are specified. For incompressible flow, relative pressure (pressure difference) rather than the absolute pressure is more important. Therefore, the pressure value at the gas outlet is set to zero. The testing domain initially is placed at zero atmospheric pressure and is filled with a given concentration of gases. For given controlled parameters, the model input parameters (listed in Table 1) can be calculated using the relations introduced in the open literature<sup>28-34</sup>. Details can be found in Wang et al.'s work<sup>14</sup>.

## 2.3 Computational Method

The multiphase flow solver InterFOAM in the OpenFOAM CFD software package<sup>35</sup> is customized so that the one-fluid formulation can be solved and coupled with the continuity, momentum, and volume fraction equations. All cases are simulated until a steady-state condition is reached. A mesh sensitivity study performed by Hu et al.<sup>11</sup> and Xu et al.<sup>36</sup> found that the mesh size of 0.1 h (h is the film thickness) is sufficient to capture the liquid film behavior. In this work, we adopt a very fine mesh of 0.0125 mm between  $x = 0$  and 1 mm (Figure 3, Section 1) to resolve the regions around the gas-liquid interface as much as possible, which is  $\sim 0.03$  h

(average film thickness  $h$  is  $\sim 0.4$  mm in this study). For regions far from the interface ( $x = 4.25$ – $5.25$  mm in Figure 3, Section 3), a coarser mesh of 0.05 mm is used. Between  $x = 1$  and 4.25 mm (Figure 3, Section 2), a total of 120 non-uniform mesh grids with a uniformly increasing ratio are employed. In the  $y$  direction, a total of 1,000 grids are uniformly distributed in the domain. A mesh dependency study is performed to investigate the impact of grid size on mass transfer coefficient. After reducing the mesh size by 50%, the simulation result ( $K_G$ ) differs only 3%, which demonstrates the grid size we adopted in this study is sufficient to predict the behavior of gas absorption across liquid film. The maximum time step size is adjusted to be  $1E-5$  seconds for the current simulation. OpenFOAM dynamically adjusts the actual time step. It takes about nine central processing unit (CPU) (AMD Interlagos 2.1 GHz) hours for 16 processors to run 1 second of the simulation.

#### 2.4 Calculation of Overall Mass Transfer Coefficient

The overall mass transfer coefficient,  $K_G$  (mol/Pa/s/m<sup>2</sup>), can be calculated via Eq. (23):

$$K_G = \frac{J}{P_{bulk}}, \quad (23)$$

where  $J$  (mol/m<sup>2</sup>/s) denotes the mass transfer flux at the gas-liquid interface and  $P_{bulk}$  (Pa) is the bulk pressure in the gas phase. Typically, the log mean driving force,  $\Delta P$ , is used to resemble the bulk pressure and can be expressed as<sup>37</sup>

$$\Delta P = \frac{(P_{CO_2,in} - P_{CO_2}^*) - (P_{CO_2,out} - P_{CO_2}^*)}{\ln \left[ \frac{P_{CO_2,in} - P_{CO_2}^*}{P_{CO_2,out} - P_{CO_2}^*} \right]}, \quad (24)$$

where  $P_{CO_2}^*$  is the equilibrium pressure. More detailed information regarding how the mass transfer coefficient is estimated can be found in<sup>38</sup>.

### 3. Simulation Results and Discussions

First, the experimental measurements of CO<sub>2</sub> absorption into the falling MEA film in a WWC device are conducted under conditions that satisfy all of the STFT assumptions as much as possible. Then, the discrepancies of  $K_G$  obtained from STFT and CFD are compared using experimental measurements as a baseline. Figure 4 illustrates the WWC design apparatus. The controlled operating input parameters and measured overall mass transfer coefficient are listed in Table 2. The mass transfer coefficients (mol/m<sup>2</sup>/s/pa) for gas film, liquid film with diffusion, and liquid film with reaction calculated from STFT correlations (Eq. (5) - (10)) for all the experimental runs are listed in Table 3. Figure 5 shows the results of case number versus experimental measurements (highlighted in black), STFT results (in red), and CFD predictions (in blue). Generally, the mass transfer coefficients predicted by STFT and numerical simulations are in good agreement with the corresponding experimental results. However, CFD predictions are slightly better for lower experimental measured mass transfer coefficients (Case 8, 15, 22, and 29), whereas STFT estimations improve at larger mass transfer (Case 23 and 25). These results suggest that both STFT and CFD results can accurately represent the actual mass transfer between gas and liquid for a steady operating WWC with laminar film.

Next, additional simulations under some extreme testing conditions are run to examine the effect of falling film instability on mass transfer coefficient by varying the frequencies of injection rate at the solvent inlet to generate surface waves. The solvent inlet velocity is described using a sinusoidal function to generate surface waves:

$$v_s = 0.1768[1 + 0.05 \sin(2\pi ft)], \quad (25)$$

where  $v_s$  denotes the solvent inlet velocity,  $t$  is time, and  $f$  represents the controlled frequency.

Testing condition is based on case No. 1 in Table 2. Four cases with different frequencies ( $f=0$

Hz, 20 Hz, 40 Hz, and 100 Hz) are tested. Figure 6 shows the profile of a falling film with varying solvent injection frequency when simulations reach the steady state. Notably, higher injection frequencies can generate more surface waves on the solvent film. Table 4 lists the increasing percentage of mass transfer coefficient at different frequencies to compare with no injection frequency results for both physical and chemical absorption of CO<sub>2</sub>. It is obvious that higher injection frequencies result in larger mass transfer coefficients because surface waves with larger frequencies create more surface area, which, in turn, enhances the gas absorption. CFD models can naturally take this effect (unstable film surface) into account (results are shown in column 2 and 3 in Table 4) because it is a physics-based model and can be implemented in different flow regime/behaviors. However, the STFT can only deal with the laminar falling film without accounting for the flow instabilities, such as ripples and waves on surfaces. In particular, the predictions from STFT will be independent of frequencies for this case as shown in the last two columns in Table 4.

To further explore the advantages of numerical simulations over STFT, the local mass transfer coefficient along the column height is investigated. Figure 7 (a) plots the streamline and flow field inside the WWC, which is rotated 90 degrees with the bottom of the WWC on the left side and its top on the right. It shows that the gas flow has a rather complex dynamical behavior, and three vortices form with two located in the lower half of the column and a slender one attached closely to the solvent film. In Figure 7 (b), the green line shows the local mass transfer coefficient variation along the column height, and the CFD results indicate that the local mass transfer coefficient can significantly differ from the overall  $K_G$  (shown as the black line). The variation in local mass transfer coefficient can be correlated to the local flow field. It has shown that the max local  $K_G$  (location 1) is about four times larger than that of the minimum  $K_G$

(location 4). The local mass transfer coefficient variation is expected because of the different  $\text{CO}_2$  concentration (or, equivalently, the driving force) along the gas-liquid interface (Figure 7 (c)) induced by the complex two-phase hydrodynamics. Four local extreme values of  $\text{CO}_2$  concentration at the gas-liquid interface (Figure 7 (c)) also turn out to be the extreme local  $K_G$  values as shown in Figure 7 (b). The results suggest that local variation of  $\text{CO}_2$  concentration results from the dynamics change of the flow regime, and higher local  $\text{CO}_2$  concentration is favorable for absorption, which increases the mass transfer coefficient. However, the STFT can yield only an overall mass transfer that does not vary locally. Our numerical simulations can provide more comprehensive details with both overall and local mass transfer information.

#### 4. Conclusion

Fully coupled multiphase flow CFD simulations with hydrodynamics, mass transfer, and chemical reactions are implemented for understanding the overall mass transfer coefficient in WWC using OpenFOAM, a free, open-source CFD software package with a custom solver. The STFT, a long-existing, widely used technique to study multiphase flow, also is thoroughly explored to represent the mass transfer resistance resulting from diffusion across laminar films. The goal is to investigate the limitations of the STFT, as well as the advantages of CFD modeling. There are several findings which include:

- 1) Both STFT and CFD results can accurately mimic the actual mass transfer between gas and liquid for a steady-operating WWC with laminar film.
- 2) The changes in mass transfer coefficient stemming from wave generation on the film surface and variation in film thickness can be captured by CFD prediction, while these flow instabilities cannot be resolved by the STFT.

- 3) Local mass transfer coefficients show dependence on dynamical variation of local velocity and concentration fields, while the STFT can only yield an overall mass transfer coefficient.

These findings indicate that the numerical prediction of mass transfer coefficient can naturally account for the dependence on the local variation of fluid velocities and properties, as well as flow instabilities, which are typically observed in the real-world WWC CO<sub>2</sub> absorption. But the impact of all those factors exceed the limits of STFT.

## 5. Acknowledgments

Pacific Northwest National Laboratory is operated by Battelle for the U.S. Department of Energy (DOE) under Contract No. DE-AC05-76RL01830. This work was funded by the DOE Office of Fossil Energy's Carbon Capture Simulation Initiative through the National Energy Technology Laboratory.

## 6. Disclaimer

This report was prepared as an account of work sponsored by an agency of the United States Government. Neither the United States Government nor any agency thereof, nor any of their employees, makes any warranty, express or implied, or assumes any legal liability or responsibility for the accuracy, completeness, or usefulness of any information, apparatus, product, or process disclosed, or represents that its use would not infringe privately owned rights. Reference herein to any specific commercial product, process, or service by trade name, trademark, manufacturer, or otherwise does not necessarily constitute or imply its endorsement, recommendation, or favoring by the United States Government or any agency thereof. The views

and opinions of authors expressed herein do not necessarily state or reflect those of the United States Government or any agency thereof.

## 7. Reference

1. Chu S, Majumdar A. Opportunities and challenges for a sustainable energy future. *Nature*. 2012 Aug 16;488(7411):294-303.
2. Herzog HJ. Peer Reviewed: What Future for Carbon Capture and Sequestration? *Environmental Science & Technology*. 2001 2001/04/01;35(7):148A-153A.
3. Whitman WG. Preliminary experimental confirmation of the two-film theory of gas absorption. *Chem Metall Eng*. 1923;29:146-149.
4. Pacheco MA, Kaganoi S, Rochelle GT. CO<sub>2</sub> absorption into aqueous mixtures of diglycolamine<sup>®</sup> and methyldiethanolamine. *Chemical Engineering Science*. 2000;55(21):5125-5140.
5. Dugas R. Carbon Dioxide Absorption, Desorption, and Diffusion in Aqueous Piperazine and Monoethanolamine: UT-Austin; 2009.
6. Dang H, Rochelle GT. CO<sub>2</sub> absorption rate and solubility in monoethanolamine/piperazine/water. *Separation science and technology*. 2003;38(2):337-357.
7. Higbie R. The rate of absorption of a pure gas into a still liquid during short periods of exposure. *Transactions of the American Institute of Chemical Engineers*. 1935 Mar;31:365-389.
8. Danckwerts PV. Significance of Liquid-Film Coefficients in Gas Absorption. *Industrial and Engineering Chemistry*. 1951;43(6):1460-1467.
9. Schlichting H, Gersten K. *Boundary-layer theory*. Springer Science & Business Media; 2003.
10. Bo SS, Ma XH, Chen HX, Lan Z. Numerical simulation on vapor absorption by wavy lithium bromide aqueous solution films. *Heat and Mass Transfer*. 2011 Dec;47(12):1611-1619.
11. Hu JG, Yang XG, Yu JG, Dai GC. Numerical simulation of carbon dioxide (CO<sub>2</sub>) absorption and interfacial mass transfer across vertically wavy falling film. *Chemical Engineering Science*. 2014 Sep 6;116:243-253.
12. Sisoiev GA, Matar OK, Lawrence CJ. Absorption of gas into a wavy falling film. *Chemical Engineering Science*. 2005 Feb;60(3):827-838.
13. Lai C, Xu Z, Pan W, Sun X, Storlie C, Marcy P, et al. Hierarchical calibration and validation of computational fluid dynamics models for solid sorbent-based carbon capture. *Powder Technology*. 2016 1//;288:388-406.
14. Wang C, Xu Z, Lai C, Whyatt G, Marcy P, Sun X. Hierarchical calibration and validation for modeling bench-scale solvent-based carbon capture. Part 1: Non-reactive physical mass transfer across the wetted wall column. *Greenhouse Gases: Science and Technology*. 2017;7(4):706-720.
15. Wang C, Xu Z, Lai K, Whyatt G, Marcy PW, Sun X. Hierarchical calibration and validation framework of bench-scale computational fluid dynamics simulations for solvent-based carbon capture. Part 2: Chemical absorption across a wetted wall column. *Greenhouse Gases: Science and Technology*. 2017:n/a-n/a.
16. Xu Z, Sun X, Khaleel MA. A generalized kinetic model for heterogeneous gas-solid reactions. *The Journal of Chemical Physics*. 2012;137(7):074702.
17. Gao D, Morley NB, Dhir V. Numerical simulation of wavy falling film flow using VOF method. *Journal of Computational Physics*. 2003 Dec 10;192(2):624-642.
18. Yu HY, Gambaryan-Roisman T, Stephan P. Numerical Simulations of Hydrodynamics and Heat Transfer in Wavy Falling Liquid Films on Vertical and Inclined Walls. *Journal of Heat Transfer-Transactions of the Asme*. 2013 Oct;135(10).

19. Haroun Y, Legendre D, Raynal L. Direct numerical simulation of reactive absorption in gas-liquid flow on structured packing using interface capturing method. *Chemical Engineering Science*. 2010 Jan 1;65(1):351-356.
20. Brackbill JU, Kothe DB, Zemach C. A Continuum Method for Modeling Surface-Tension. *Journal of Computational Physics*. 1992 Jun;100(2):335-354.
21. Astarita G, Savage DW, Bistrot A. *Gas Treating with Chemical Solvents*. New York: John Wiley & Sons.; 1983.
22. Blauwhoff PMM, Versteeg GF, Van Swaaij WPM. A study on the reaction between CO<sub>2</sub> and alkanolamines in aqueous solutions. *Chemical Engineering Science*. 1984 1984/01/01;39(2):207-225.
23. Danckwerts PV. *Gas-Liquid Reactions*. McGraw-Hill Book Company; 1970.
24. Danckwerts PV. The reaction of CO<sub>2</sub> with ethanolamines. *Chemical Engineering Science*. 1979 1979/01/01;34(4):443-446.
25. Versteeg GF, van Swaaij WPM. On the kinetics between CO<sub>2</sub> and alkanolamines both in aqueous and non-aqueous solutions—I. Primary and secondary amines. *Chemical Engineering Science*. 1988 1988/01/01;43(3):573-585.
26. Ali SH. Kinetics of the reaction of carbon dioxide with blends of amines in aqueous media using the stopped-flow technique. *International Journal of Chemical Kinetics*. 2005 Jul;37(7):391-405.
27. Gabrielsen J, Michelsen ML, Stenby EH, Kontogeorgis GM. A model for estimating CO<sub>2</sub> solubility in aqueous alkanolamines. *Industrial & Engineering Chemistry Research*. 2005 Apr 27;44(9):3348-3354.
28. Cussler EL. *Diffusion: Mass Transfer in Fluid Systems*. 2nd ed; New York: Cambridge University Press; 1997.
29. Fu D, Xu YF, Wang LF, Chen LH. Experiments and model for the surface tension of carbonated monoethanolamine aqueous solutions. *Science China-Chemistry*. 2012 Jul;55(7):1467-1473.
30. Khan FM, Mahmud T. In: *Modelling of Gas Absorbers for Carbon Dioxide Capture Applications*.
31. Li MH, Lai MD. Solubility and Diffusivity of N<sub>2</sub>O and CO<sub>2</sub> in (Monoethanolamine Plus N-Methyldiethanolamine Plus Water) and in (Monoethanolamine Plus 2-Amino-2-Methyl-1-Propanol Plus Water). *Journal of Chemical and Engineering Data*. 1995 Mar-Apr;40(2):486-492.
32. Snijder ED, Teriele MJM, Versteeg GF, Vanswaaij WPM. Diffusion-Coefficients of Several Aqueous Alkanolamine Solutions. *Journal of Chemical and Engineering Data*. 1993 Jul;38(3):475-480.
33. Weiland RH, Dingman JC, Cronin DB, Browning GJ. Density and viscosity of some partially carbonated aqueous alkanolamine solutions and their blends. *Journal of Chemical and Engineering Data*. 1998 May-Jun;43(3):378-382.
34. Wilke CR. A Viscosity Equation for Gas Mixtures. *Journal of Chemical Physics*. 1950;18(4):517-519.
35. OpenFOAM – Open source Field Operation And Manipulation. Version OpenFOAM 2.2.0. Download available <http://www.openfoam.org/download/>.
36. Xu ZF, Khoo BC, Wijesundera NE. Mass transfer across the falling film: Simulations and experiments. *Chemical Engineering Science*. 2008 May;63(9):2559-2575.
37. Cullinane JT. *Thermodynamics and Kinetics of Aqueous Piperazine with Potassium Carbonate for Carbon Dioxide Absorption*. [Austin, Texas]: The University of Texas at Austin; 2005.
38. Wang C, Xu Z, Lai C, Whyatt G, Marcy P, Gattiker J, et al. PNNL Report on the Development of Bench-scale CFD Simulations for Gas Absorption across a Wetted Wall Column Richland, WA; 2016.

## Figures

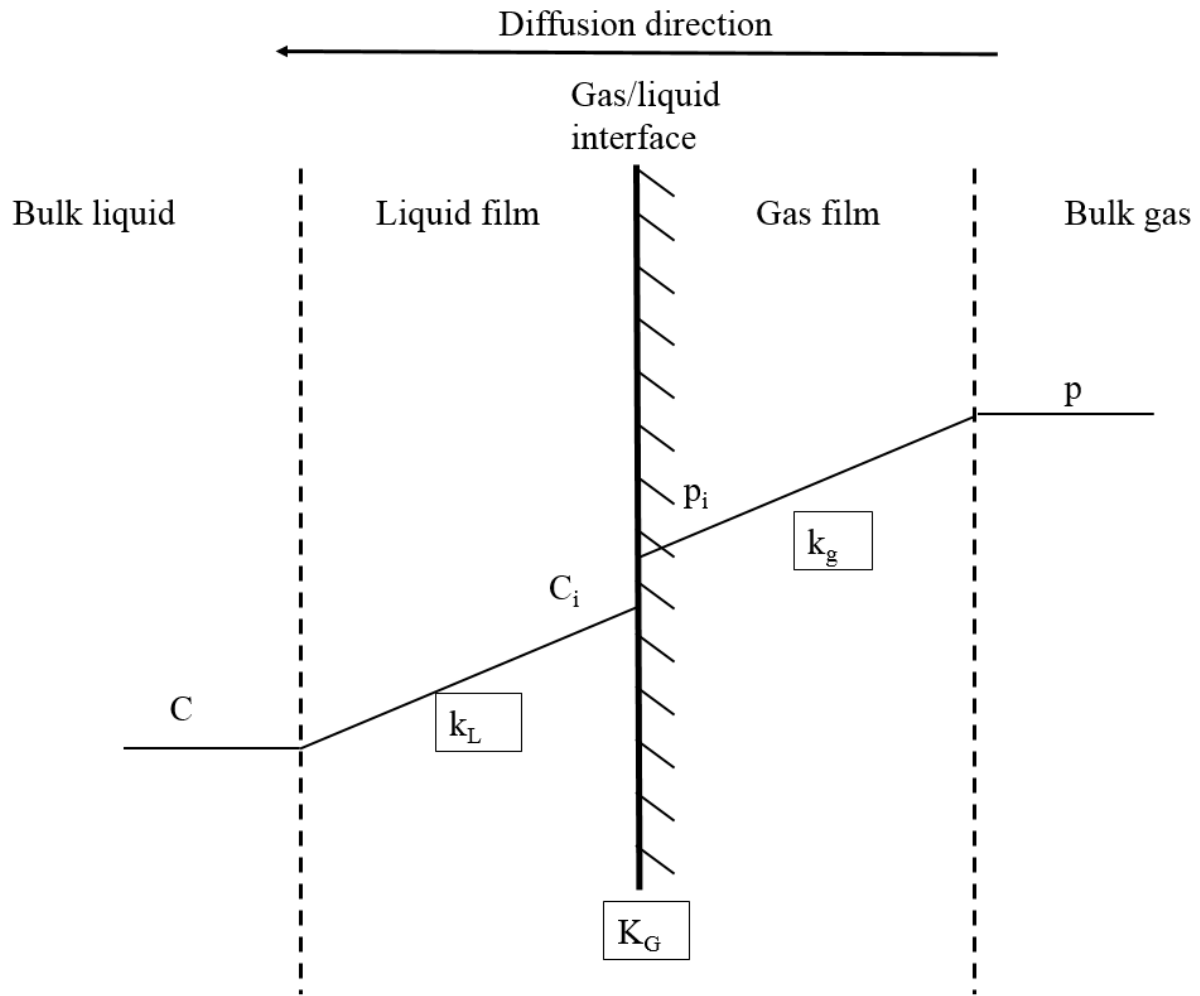


Figure 1 STFT Schematic Representation

ACCEPTED

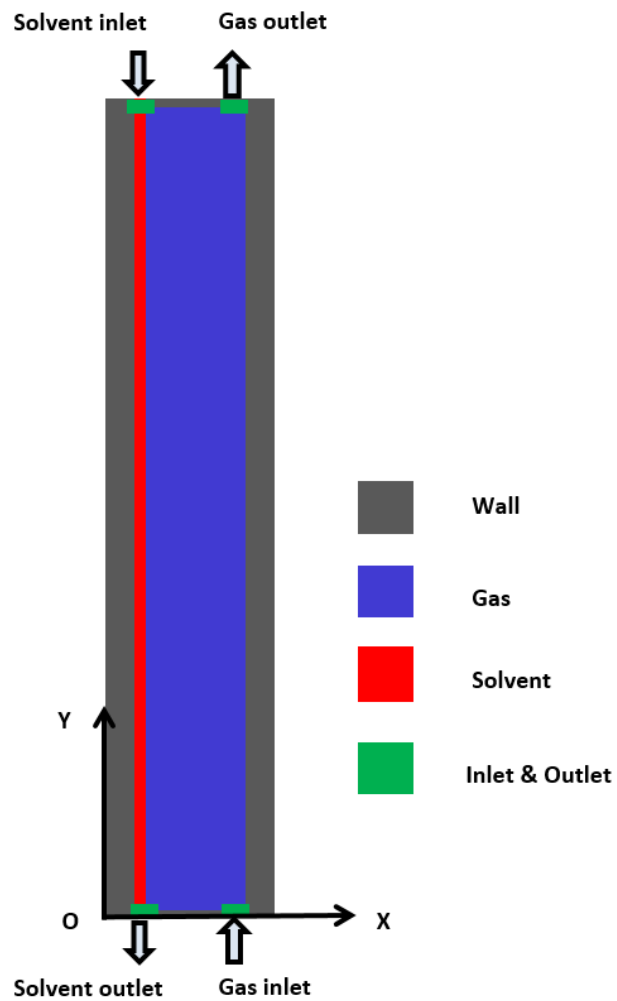
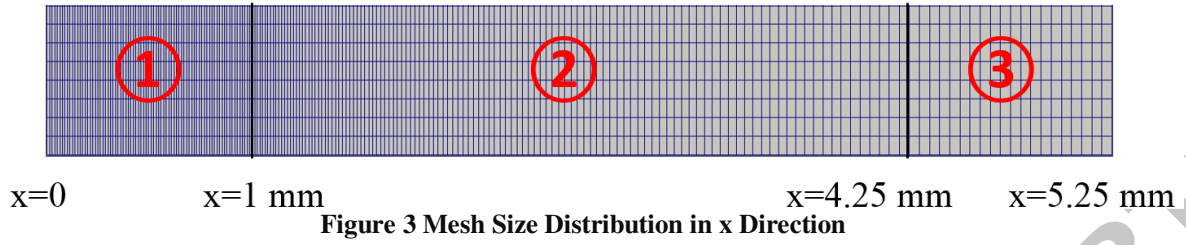
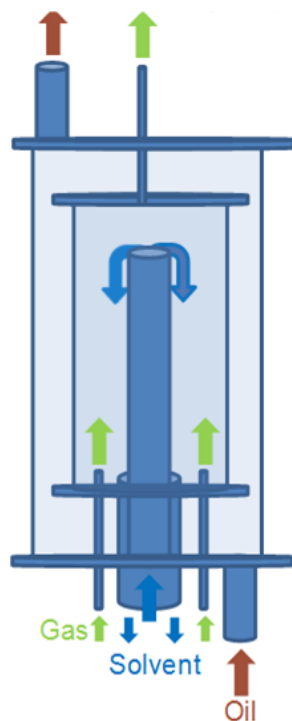


Figure 2 Countercurrent Gas Flow Geometry Schematics





**Figure 4 WWC Schematic.** Gas enters the chamber through three 1/8-inch tubes spaced evenly around the circumference of the annulus and exits through a 1/4-inch tube at the top of the column. Solvent flows up the center of the tube and falls down over the outside of the tube. Oil at the test temperature surrounds the inner chamber to maintain the desired test temperature.

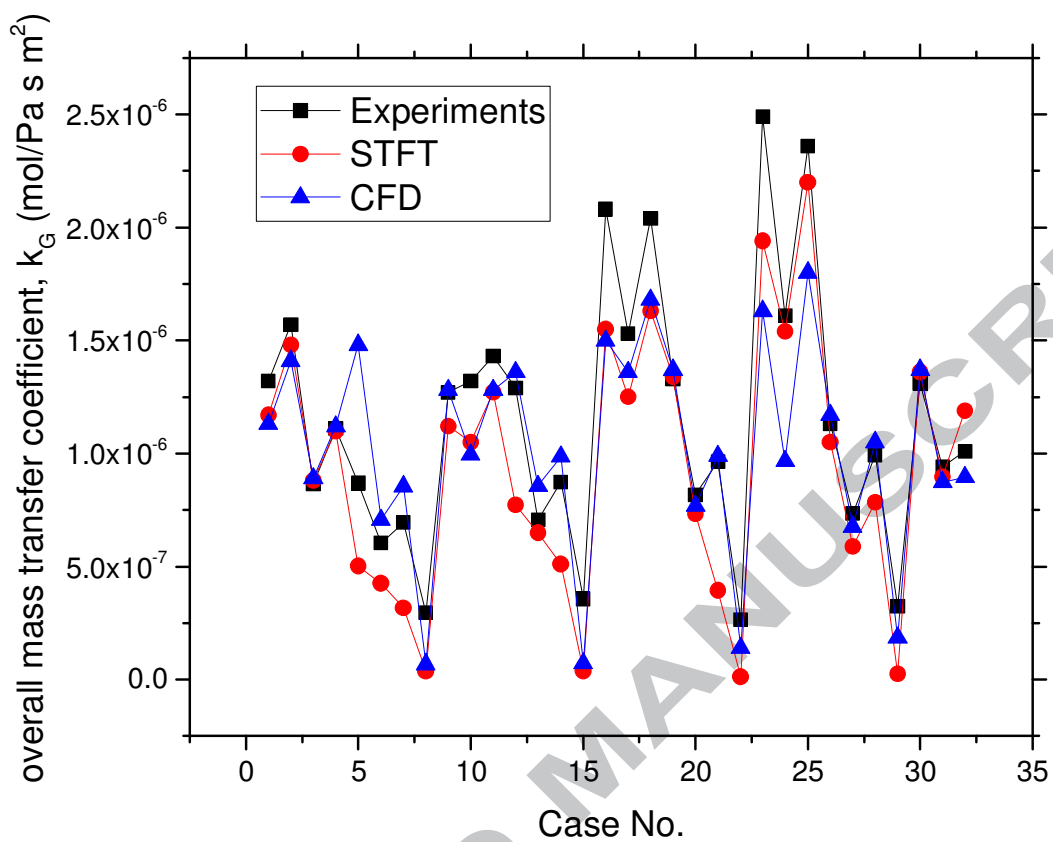
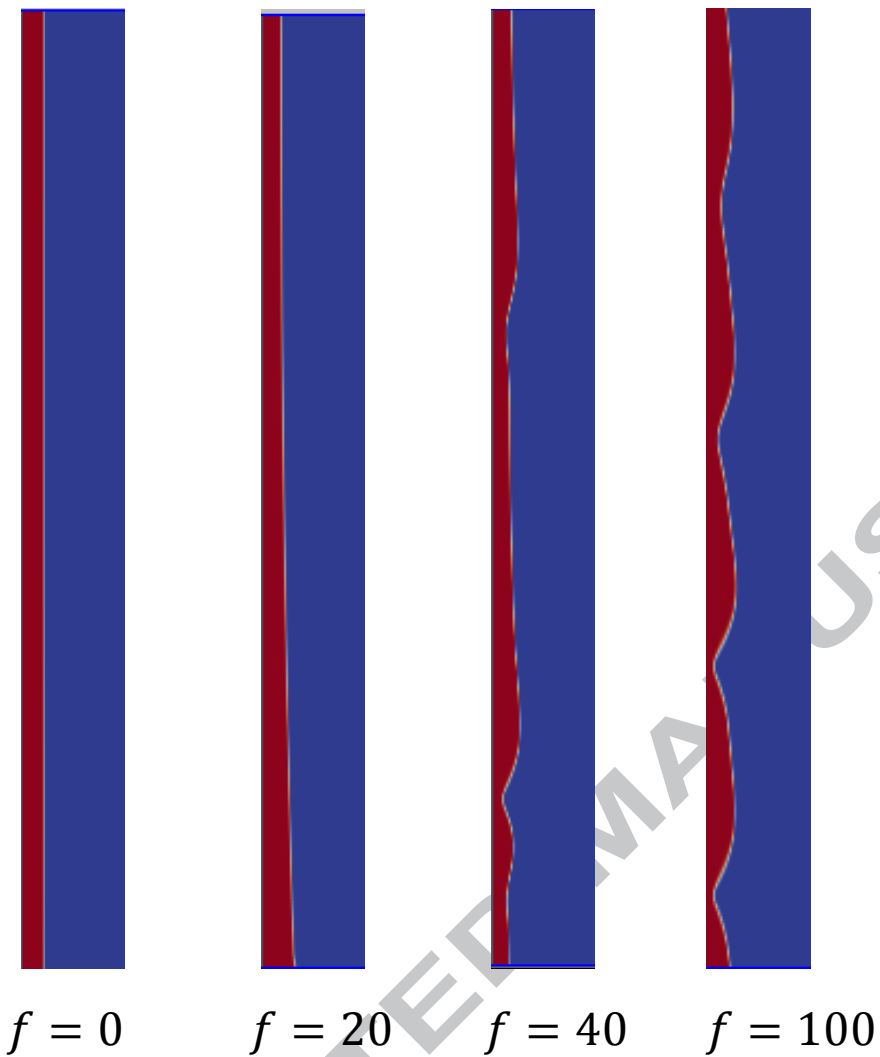
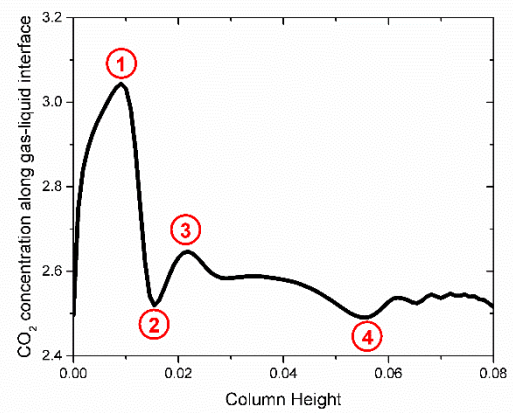
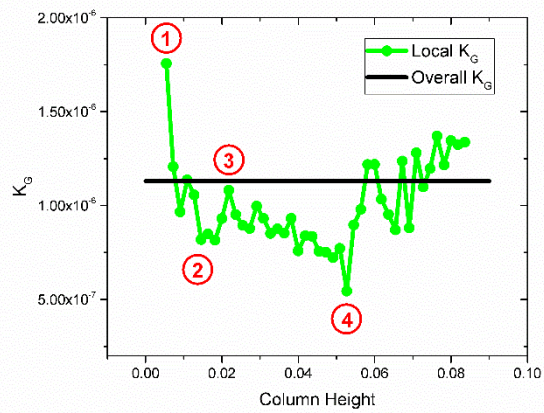
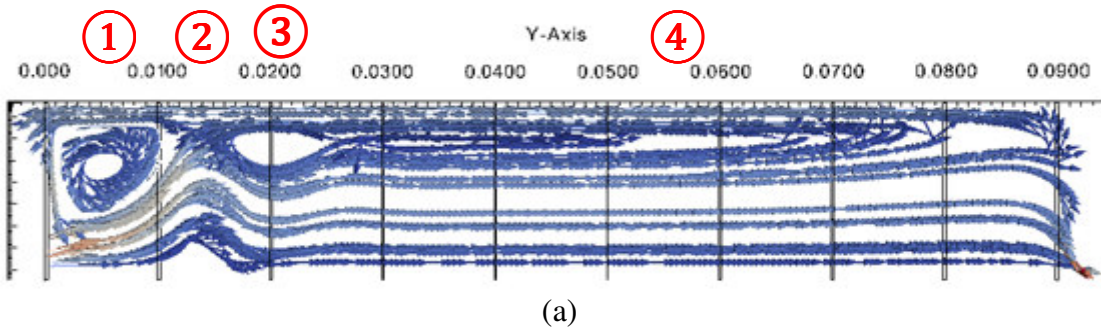


Figure 5 Numerical Simulation and STFT Results versus Experimental Data for Overall Mass Transfer Coefficient in the CO<sub>2</sub>/MEA System. The numerical and STFT results match reasonably well with experimental results.



**Figure 6 Effect of frequencies on surface waves. Increasing injection frequencies can generate more surface waves. CFD simulation can predict the influence of surface waves on the mass transfer coefficient, while STFT cannot deal with flow instabilities.**



**Figure 7 Local Mass Transfer Coefficient: (a) Streamline and Flow Field; (b) Local  $K_G$  versus Overall  $K_G$ ; (c)  $\text{CO}_2$  Concentration ( $\text{mol}/\text{m}^3$ ) Along Gas-Liquid Interface. Testing condition is based on case No. 1 in Table 2.**

**Tables****Table 1 Direct Model Input Parameters**

| Parameters                         | Unit                    |
|------------------------------------|-------------------------|
| Solvent inlet velocity             | m/s                     |
| Gas inlet velocity                 | m/s                     |
| Inlet concentration (solvent, gas) | mol/m <sup>3</sup>      |
| Diffusivity (solvent, gas)         | m <sup>2</sup> /s       |
| Gas diffusivity in solvent         | m <sup>2</sup> /s       |
| Solvent contact angle              | degree                  |
| Density (solvent, gas)             | kg/m <sup>3</sup>       |
| Kinematic viscosity (solvent, gas) | m <sup>2</sup> /s       |
| Surface tension                    | kg/s <sup>2</sup>       |
| Henry's constant                   | Dimensionless           |
| Reaction rate constant             | m <sup>3</sup> /(mol·s) |

**Table 2 CO<sub>2</sub>/MEA Controlled Input Parameters and Measured Overall Mass Transfer Coefficient**

| Run # | MEA mass fraction | CO <sub>2</sub> loading (mol CO <sub>2</sub> /mol MEA) | Solvent flow rate, cc/min | Gas flow rate, sccm | CO <sub>2</sub> molar fraction | Temp. °C | K <sub>G</sub> , mol/(Pa·s·m <sup>2</sup> ) |
|-------|-------------------|--|---------------------------|---------------------|--------------------------------|----------|---|
| 1     | 0.25              | 0.30   | 450                       | 4000                | 0.115                          | 42       | 1.32E-06                                    |
| 2     | 0.10              | 0.10   | 495                       | 4344                | 0.070                          | 45       | 1.57E-06                                    |
| 3     | 0.10              | 0.20   | 590                       | 2126                | 0.191                          | 27       | 8.64E-07                                    |
| 4     | 0.10              | 0.20   | 352                       | 2724                | 0.086                          | 49       | 1.11E-06                                    |
| 5     | 0.10              | 0.30   | 550                       | 2558                | 0.164                          | 55       | 8.69E-07                                    |
| 6     | 0.10              | 0.40   | 318                       | 2284                | 0.183                          | 47       | 6.04E-07                                    |
| 7     | 0.10              | 0.40   | 404                       | 3474                | 0.158                          | 59       | 6.94E-07                                    |
| 8     | 0.10              | 0.50   | 558                       | 2681                | 0.056                          | 32       | 2.95E-07                                    |
| 9     | 0.20              | 0.10   | 322                       | 2342                | 0.032                          | 30       | 1.27E-06                                    |
| 10    | 0.20              | 0.20   | 426                       | 3735                | 0.142                          | 31       | 1.32E-06                                    |
| 11    | 0.20              | 0.20   | 466                       | 3899                | 0.064                          | 38       | 1.43E-06                                    |
| 12    | 0.20              | 0.30   | 338                       | 5549                | 0.134                          | 53       | 1.29E-06                                    |
| 13    | 0.20              | 0.40   | 410                       | 3345                | 0.127                          | 43       | 7.06E-07                                    |
| 14    | 0.20              | 0.40   | 475                       | 3635                | 0.043                          | 56       | 8.74E-07                                    |
| 15    | 0.20              | 0.50   | 521                       | 2861                | 0.147                          | 39       | 3.56E-07                                    |
| 16    | 0.30              | 0.10   | 363                       | 4682                | 0.106                          | 41       | 2.08E-06                                    |
| 17    | 0.30              | 0.20   | 532                       | 5130                | 0.175                          | 33       | 1.53E-06                                    |
| 18    | 0.30              | 0.20   | 375                       | 5241                | 0.049                          | 56       | 2.04E-06                                    |
| 19    | 0.30              | 0.30   | 488                       | 3107                | 0.110                          | 52       | 1.33E-06                                    |
| 20    | 0.30              | 0.40   | 432                       | 4189                | 0.102                          | 41       | 8.17E-07                                    |
| 21    | 0.30              | 0.40   | 458                       | 4839                | 0.079                          | 51       | 9.64E-07                                    |
| 22    | 0.30              | 0.50   | 308                       | 5991                | 0.196                          | 25       | 2.65E-07                                    |
| 23    | 0.40              | 0.10   | 537                       | 4431                | 0.116                          | 46       | 2.49E-06                                    |
| 24    | 0.40              | 0.20   | 513                       | 4066                | 0.121                          | 36       | 1.61E-06                                    |
| 25    | 0.40              | 0.20   | 570                       | 5673                | 0.179                          | 59       | 2.36E-06                                    |
| 26    | 0.40              | 0.30   | 378                       | 5301                | 0.040                          | 34       | 1.13E-06                                    |
| 27    | 0.40              | 0.40   | 588                       | 5790                | 0.093                          | 28       | 7.34E-07                                    |
| 28    | 0.40              | 0.40   | 449                       | 4869                | 0.153                          | 49       | 9.93E-07                                    |
| 29    | 0.40              | 0.50   | 395                       | 3189                | 0.078                          | 37       | 3.23E-07                                    |
| 30    | 0.25              | 0.30   | 450                       | 4000                | 0.115                          | 42       | 1.31E-06                                    |
| 31    | 0.10              | 0.20   | 590                       | 2126                | 0.191                          | 27       | 9.41E-07                                    |
| 32    | 0.40              | 0.40   | 449                       | 4869                | 0.153                          | 49       | 1.01E-06                                    |

**Table 3 Mass transfer coefficients (mol/m<sup>2</sup>/s/pa) for gas film, liquid film with diffusion, and liquid film with reaction obtained from STFT correlations**

| Run # | Gas phase mass transfer coefficient from STFT | Liquid phase mass transfer coefficient with diffusion only from STFT | Liquid phase mass transfer coefficient with reaction from STFT |
|-------|---|--|--|
| 1     | 7.04E-06                                      | 2.60E-08   | 1.40E-06   |
| 2     | 7.48E-06                                      | 3.63E-08   | 1.84E-06   |
| 3     | 4.32E-06                                      | 4.23E-08   | 1.10E-06   |
| 4     | 4.97E-06                                      | 2.68E-08   | 1.40E-06   |
| 5     | 4.62E-06                                      | 2.66E-08   | 5.63E-07   |
| 6     | 4.30E-06                                      | 2.53E-08   | 4.72E-07   |
| 7     | 5.92E-06                                      | 1.95E-08   | 3.35E-07   |
| 8     | 5.17E-06                                      | 3.69E-08   | 3.60E-08   |
| 9     | 4.64E-06                                      | 2.61E-08   | 1.46E-06   |
| 10    | 6.88E-06                                      | 2.71E-08   | 1.23E-06   |
| 11    | 6.98E-06                                      | 2.93E-08   | 1.55E-06   |
| 12    | 8.98E-06                                      | 2.20E-08   | 8.45E-07   |
| 13    | 6.03E-06                                      | 2.63E-08   | 7.27E-07   |
| 14    | 6.21E-06                                      | 1.98E-08   | 5.56E-07   |
| 15    | 5.35E-06                                      | 2.57E-08   | 3.77E-08   |
| 16    | 8.07E-06                                      | 2.18E-08   | 1.92E-06   |
| 17    | 8.95E-06                                      | 2.64E-08   | 1.45E-06   |
| 18    | 8.48E-06                                      | 2.05E-08   | 2.02E-06   |
| 19    | 5.50E-06                                      | 2.71E-08   | 1.72E-06   |
| 20    | 7.35E-06                                      | 2.25E-08   | 8.13E-07   |
| 21    | 8.05E-06                                      | 1.86E-08   | 4.14E-07   |
| 22    | 1.05E-05                                      | 2.02E-08   | 1.20E-08   |
| 23    | 7.58E-06                                      | 2.55E-08   | 2.60E-06   |
| 24    | 7.28E-06                                      | 2.79E-08   | 1.94E-06   |
| 25    | 8.99E-06                                      | 2.62E-08   | 2.90E-06   |
| 26    | 9.18E-06                                      | 2.02E-08   | 1.18E-06   |
| 27    | 1.01E-05                                      | 2.10E-08   | 6.25E-07   |
| 28    | 8.14E-06                                      | 1.72E-08   | 8.68E-07   |
| 29    | 5.90E-06                                      | 2.11E-08   | 2.52E-08   |
| 30    | 7.04E-06                                      | 3.13E-08   | 1.68E-06   |
| 31    | 4.32E-06                                      | 4.35E-08   | 1.13E-06   |
| 32    | 8.14E-06                                      | 2.82E-08   | 1.38E-06   |

**Table 4 Mass Transfer Coefficient Changes with Frequency for Both Physical and Chemical Absorption of CO<sub>2</sub>**

| Frequency,<br><i>f</i> | Increase, %  |  |  |  |
|------------------------|--|--|--|--|
|                        | CFD  |  | STFT   |  |
|                        | Physical absorption,<br>$K_G=2.37E-8$<br>mol/m <sup>2</sup> /s/Pa at $f=0$ | Chemical absorption,<br>$K_G=1.13E-6$<br>mol/m <sup>2</sup> /s/Pa at $f=0$ | Physical absorption,<br>$K_G=1.60E-8$<br>mol/m <sup>2</sup> /s/Pa at $f=0$ | Chemical absorption,<br>$K_G=1.17E-6$<br>mol/m <sup>2</sup> /s/Pa at $f=0$ |
| 20                     | 11.39  | 7.08   | 0  | 0  |
| 40                     | 21.10  | 12.39  | 0  | 0  |
| 100                    | 37.55  | 19.46  | 0  | 0  |